Mottness collapse without metallization in the domain wall of the triangular-lattice Mott insulator $1T-TaS_2$

Jan Skolimowski,[1] Yaroslav Gerasimenko,[2] and Rok Žitko[1,3]
[1]*Jožef Stefan Institute, Jamova 39, SI-1000 Ljubljana, Slovenia*
[2]*CENN Nanocenter, Jamova 39, SI-1000 Ljubljana, Slovenia*
[3]*Faculty of Mathematics and Physics, University of Ljubljana, Jadranska 19, SI-1000 Ljubljana, Slovenia*

(Received 8 June 2018; revised manuscript received 22 October 2018; published 25 January 2019)

$1T-TaS_2$ is a charge-density-wave (CDW) compound with a Mott-insulating ground state. The metallic state obtained by doping, substitution, or pulsed charge injection is characterized by an emergent CDW domain-wall network, while single domain walls can be found in the pristine Mott state. Here we study whether and how the single walls become metallic. Tunneling spectroscopy reveals partial suppression of the Mott gap and the presence of in-gap states strongly localized at the domain-wall sites. Using the real-space dynamical mean field theory description of the strongly correlated quantum-paramagnet ground state, we show that the local gap suppression follows from the increased hopping along the connected zigzag chain of lattice sites forming the domain wall. Furthermore, we show that full metallization is preempted by the splitting of the quasiparticle band into bonding and antibonding subbands due to the structural dimerization of the wall, explaining the presence of the in-gap states and the low density of states at the Fermi level.

DOI: 10.1103/PhysRevLett.122.036802

The interplay between superconductivity (SC) and correlated insulating phases, such as Mott insulators and charge density waves (CDWs), is one of the central problems in condensed-matter physics. Remarkably, their combination can be found even in simple material systems, such as the transition metal dichalcogenide (TMD) van der Waals compound $1T-TaS_2$. The ground state is a Mott insulator [1–3] with CDWs [4] and unconventional quantum spin liquid behavior [5–10]. Upon Se substitution [11], Fe intercalation [12], or by applying pressure [13] it becomes superconducting, with both CDWs and correlated behavior still present. Further control over electronic properties is possible through nonequilibrium charge injection via ultrafast optical or electrical pulses [14–21], which lead to drastic insulator to metastable metal transition. The long-standing hypothesis for metallization and SC onset is linked to the formation of CDW domain walls, seen in multiple TMDs with different techniques [22–24]. Recently, it was challenged experimentally with scanning tunneling spectroscopy (STS) [25], which showed the absence of metallization in certain types of walls. First-principles calculations revealed that atomic reconstruction in the walls may cause the formation of bound states [25] and band reconstruction [24], but the correlation effects were left out of scope. Thus, the crucial question of whether the CDW distortion inside the wall can lead to Mottness collapse remains open. In this Letter, we combine STS and dynamical mean field theory (DMFT) calculations to study the behavior of the Mott gap in CDW domain walls, finding Mottness collapse without metallization.

In $1T-TaS_2$, each layer is periodically modulated to form a $\sqrt{13}\times\sqrt{13}$ superlattice of David star deformations [4], resulting in a commensurate CDW state with a single half filled electron band at the Fermi level [26,27]. The Coulomb repulsion opens a charge gap in this band, resulting in a Mott-insulating ground state [2,28–31]. Single CDW domain walls (DWs) [17,25,32] can be found connecting large lattice inhomogeneities in freshly cleaved samples or they remain after the relaxation of the metastable metallic mosaic state created with voltage pulse from the scanning tunneling microscope (STM) tip. We study both examples and find the relevant physics similar.

The topographic STM image in Fig. 1(a) reveals individual David stars as bright spots packed in a triangular lattice. The DW is seen as a misfit of the lattices on left and right sides: David stars partially overlap and are shifted with respect to each other. Among the 12 possible DW types, only a few are observed experimentally [17]: indeed, in the most commonly seen DWs, the stars are drawn closer together [Fig. 1(b)], but still retain their shape; see Supplemental Material for an extended discussion [33]. The DW is very localized, approximately two superlattice constants in extent, so that its core roughly consists of a 1D zigzag chain of the nearest-neighbor stars [Fig. 1(c)].

The tunneling spectra [Fig. 1(d)] reveal the apparent Mott gap closing at the DW, while the clear bending of the Hubbard bands outside the DW indicates its charging. The CDW gap is quite robust, except at the very center of the DW. Changes to the Mott gap occur on significantly

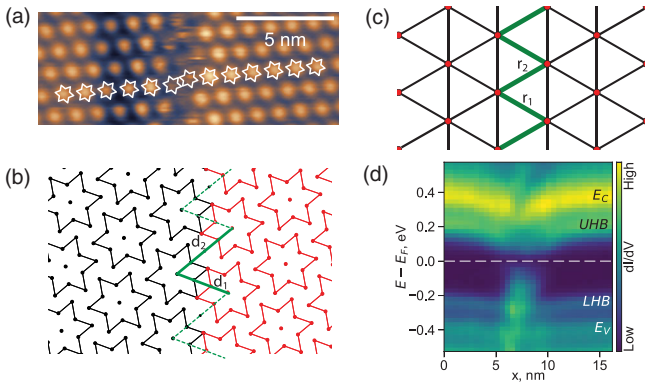

FIG. 1. Domain walls in $1T-TaS_2$. (a) STM topographic image of a single domain wall separating two adjacent CDW domains ($V_{\rm tip} = -0.8$ V, $I = 100$ pA, $T = 4.2$ K). (b) Schematic diagram of the configuration of David stars near the domain wall: the stars along the wall are brought closer together. The modified center-to-center distances are indicated as d_1, d_2. (c) Hubbard model description of the domain wall: one-dimensional zigzag chain with modified hoppings (ratios r_1, r_2, green line) embedded in a two-dimensional Mott-insulator environment. (d) dI/dV map across the domain wall (domain wall A, DW-A, averaged over longitudinal direction). LHB and UHB are lower and upper Hubbard bands, E_c and E_v indicate the additional conducting and valence bands associated with the Ta d shell.

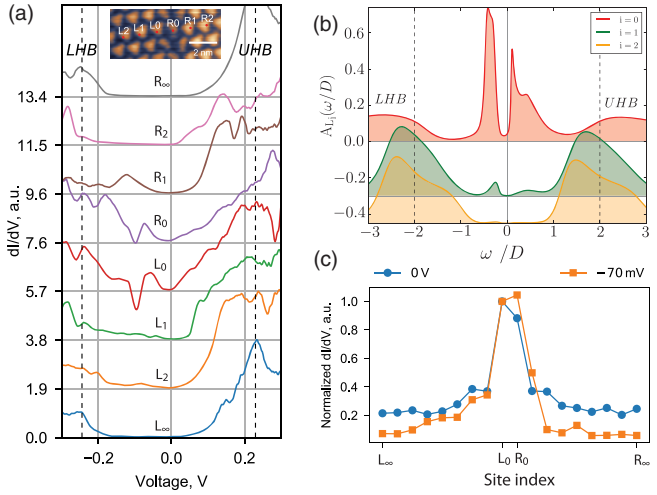

FIG. 2. Subgap features in the domain wall. (a) Position-resolved dI/dV tunneling spectra across the domain wall B (DW-B). L_i and R_i indicate left and right side; i counts the distance from the domain-wall center in units of supercells. The spectra are offset for clarity, the horizontal grid lines correspond to $dI/dV = 0$ level for each curve. (b) Theoretical prediction for the spectra at the domain wall and in its vicinity. (c) Cross sections of spectra at selected voltages: at Fermi level (blue line, $V = 0$) and at the in-gap level (orange line, $V = -70$ meV). Spectra are normalized to the value at the point L_1.

larger spatial scales, allowing us to decouple the two gaps. The spectral weight is distributed unevenly along the DW (see Supplemental Material [33]), suggesting finite scattering. Closer inspection of the high-resolution density of states (DOS) in the Mott gap, done on another DW sector, shows two more major features: (i) inside the DW, the DOS is significantly reconstructed and a small nonzero weight appears at the Fermi level, and (ii) in-gap states at -70 mV are present on top of a smooth spectrum [see Fig. 2(a)].

We now construct an effective model to understand the observed low-energy behavior in the DW. The minimal model for the Mott state in TaS_2 is the single-band Hubbard model on a triangular lattice at half filling [29,30,42–46],

$$H = \sum_{\langle i,j\rangle,\sigma} t_{ij} c^{\dagger}_{i\sigma} c_{j\sigma} + \sum_{i\sigma} \epsilon_i n_{i\sigma} + \sum_i U_i n_{i\uparrow} n_{i\downarrow}, \quad (1)$$

where i,j are site indices, $\sigma = \uparrow, \downarrow$ is spin, $c^{\dagger}_{i\sigma}$ are electron creation operators, $n_{i\sigma} = c^{\dagger}_{i\sigma} c_{i\sigma}$ are the local electron-occupancy operators, t_{ij} are the hopping constants between nearest neighbors, ϵ_i are the on site potentials, and U_i are the Hubbard repulsion parameters. Down to the lowest temperatures, TaS_2 does not order magnetically [6,9]. A simple approximation to describe this experimentally observed paramagnetic Mott-insulating state, theoretically predicted to exist in a range of U between the paramagnetic metal and the 120° Néel ordered state [47,48], is the DMFT [29,49]. This approach can be generalized to the inhomogeneous case [50–59]. Here we assume the DW lattice structure to be predetermined and fixed, and we focus on the effects of such a deformation on the electronic degrees of freedom.

The modified separation between the stars in the DW is reflected in a change of the corresponding hopping constants t_{ij} due to a different overlap of the corresponding Wannier wave functions; see the adjacent black and red stars in Fig. 1(b), represented by the green line in Fig. 1(c). The rescale factor for the hopping constants will be denoted as r. (In unperturbed bulk $t_{ij} \equiv t$, while $t_{ij} = rt$ for i, j belonging to the DW.) The superlattice deformation along the DW has a longitudinal component, leading to a period-2 modulation of r along the DW (the values will be denoted by r_1 and r_2). Next, we allow for a modification of the on site energies ϵ_i resulting from the deformation of the stars. The additional on site potential at the DW sites will be denoted as δ. For simplicity, we assume that the Hubbard constants remain uniform, $U_i \equiv U$. We set $U = 4D$, where $2D = 9t$ is the bandwidth of the triangular-lattice DOS. We fix the chemical potential in the center of the bulk Mott gap. We now study the effects of the inhomogeneity on the local DOS (LDOS) using the real-space DMFT approach as described in the Supplemental Material [33]. The main result is that in the DW the Mott state collapses if at least one of r_1, r_2 is large enough, due to an increase in the kinetic energy of the DW subsystem; however, the resulting state has a low Fermi-level LDOS for $r_1 \neq r_2$ due to the splitting of the quasiparticle band into bonding and antibonding subbands, which tends to open a (pseudo) gap.

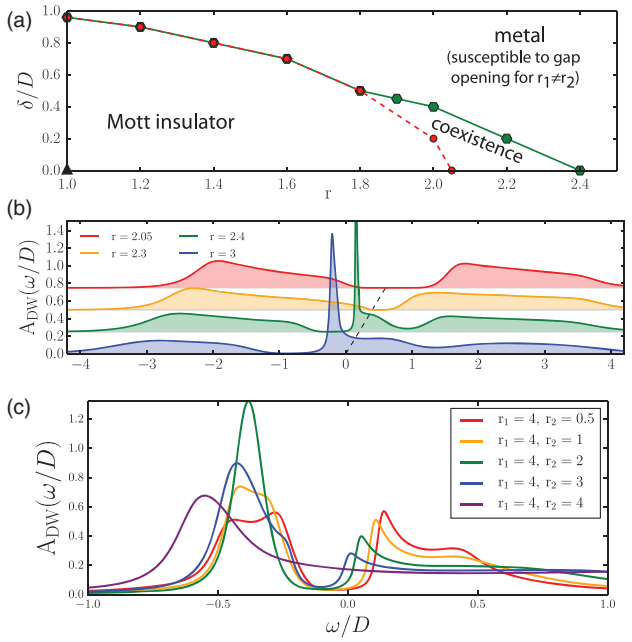

FIG. 3. Insulating and metallic regimes. (a) Phase diagram of the domain-wall subsystem as a function of the hopping enhancement factor $r \equiv r_1 = r_2$ and the local potential δ. (b) Domain-wall spectral function across the bandwidth-driven Mott transition. (c) Effects of the dimerization, $r_1 \neq r_2$, on the quasiparticle band in a metallic wall.

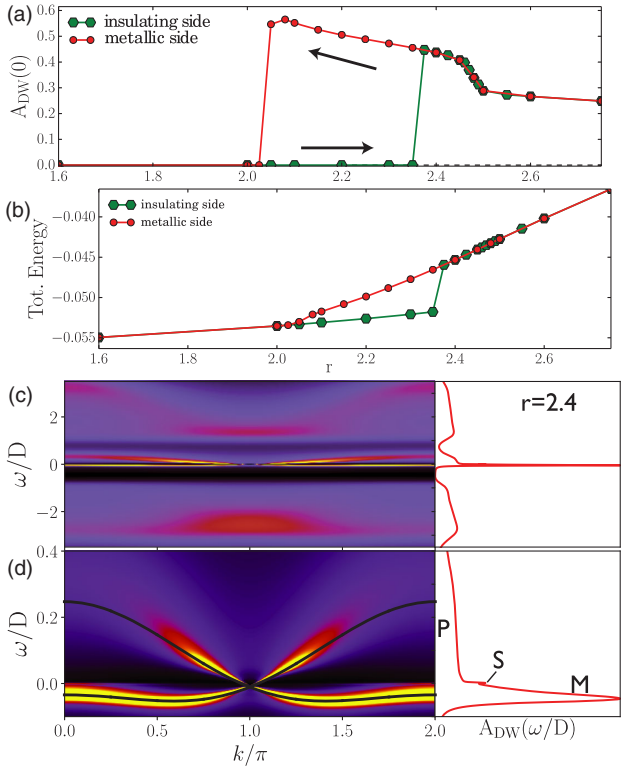

FIG. 4. Effects of the hopping enhancement factor r with δ fixed at 0. (a) Local DOS at the Fermi level across the bandwidth-driven Mott transition. The arrows in the hysteresis region indicate the direction of the changing parameter r. (b) Total energies of metallic and insulating solutions. (c),(d) Momentum-resolved spectral functions. k is the momentum along the DW. The black line is the dispersion of a noninteracting 1D zigzag chain tight-binding Hamiltonian.

In $1T - TaS_2$, the lattice geometry effects are particularly important: the zigzag nature of the lattice distortion makes the DW a connected linear system embedded in a bulk Mott-insulator sheet. The homogeneous Hubbard model undergoes Mott metal-insulator transitions (MITs) of two types [42,49,60–64]: interaction- and bandwidth-driven (Hubbard repulsion U overcomes the kinetic energy proportional to hopping) or doping-driven (for sufficiently large U the electron-occupancy approaches half filling). If the system lacks translation invariance, the MIT can also take place in a subsystem, e.g., on a surface, at an interface, or in a domain wall [50–54]. In TaS_2, the DW subsystem metallizes if $r_1 = r_2 \equiv r$ becomes large (bandwidth-driven MIT) or if δ becomes large (doping-driven MIT) [see Fig. 3(a)].

The "local charge gap" is reduced inside the DW. This is due to the enhanced hopping r that increases the effective bandwidth so that local lower and upper Hubbard bands (LHB and UHB, respectively) become broader, while the band centers shift only a little. Because of the particle-hole asymmetry in the triangular lattice, the top of LHB and the bottom of UHB have quite different shapes, and the upper edge of the LHB moves towards the Fermi level with increasing r faster than the bottom edge of the UHB. For high enough $r = r_1 = r_2$, the DW goes through a MIT and it metallizes: a quasiparticle (QP) band emerges inside the Mott gap [Fig. 3(b)] so that the Fermi-level local LDOS jumps to a finite value [Fig. 4(a)]. The QP band has a highly asymmetric internal structure with a sharp maximum M in the occupied part of the spectrum (the maximum is not pinned to the Fermi level) and an extended flat plateau P in the unoccupied part [see Fig. 4(d), right panel]. In addition, in the range $r \lesssim 2.5$ we find a weak secondary peak S (see Supplemental Material for its interpretation [33]). Information about the in-gap states can be extracted from the momentum-resolved (partially Fourier transformed) spectral function $A_{k,i}(\omega)$, where k is the longitudinal momentum in the DW direction, while i is the index of the DW site in the transverse direction. An overview is shown in Fig. 4(c), and a closeup to the QP band is shown in Fig. 4(d). The dominant features (M and P) in the structure of the QP band are due to the one-dimensional nature of the DW, which is a 1D zigzag chain with nearest and next-nearest neighbor hopping constants differing by a factor of r. The band dispersion for such a noninteracting tight-binding model with $r = 2.4$ indeed matches the QP dispersion [Fig. 4(d)].

Surprisingly, the boundary bandwidth-driven MIT is first order even at zero temperature, unlike the bulk MIT. We find a sizeable region with coexisting DMFT solutions:

with increasing r, the insulating solution metallizes at $r_{c,2}$, while with decreasing r the metallic solution becomes insulating at $r_{c,1} < r_{c,2}$. The insulating solution is stable in the entire coexistence region, $r_{c,1} < r < r_{c,2}$ [Fig. 4(b)]. As a consequence, the bandwidth-driven transition from the insulating state happens at the moment when the Hubbard band (here LHB) touches the chemical potential, similar to the scenario for the disappearance of the metastable insulating DMFT solution in the bulk case. We note, however, that for $r > r_{c,2}$ the LHB becomes clearly separated from the QP peak; i.e., at $r = r_{c,2}$ the LDOS changes discontinuously. The doping-driven boundary Mott transition also proceeds by the mechanism of LHB crossing the chemical potential, but the QP peak is pinned to the top of the LHB right after the transition (see Supplemental Material for more details [33]).

The superlattice deformation at the DW corresponds to an increase of hopping that can easily attain values of $r \approx 3$ or 4 (see Supplemental Material for estimates corresponding to common DW types [33]). One would thus generically expect to observe a strong metallization and a prominent peak at (or close to) the Fermi level. In reality, however, the DW is naturally dimerized so that $r_1 \neq r_2$. For most DW types, r_1 and r_2 can indeed be quite different. The Mott phase collapses at the DW if the kinetic energy of the 1D subsystem is high enough. For this to occur, it is sufficient for one of r_1, r_2 to be large, even if the 1D subsystem in isolation from the triangular-lattice bulk would actually be gapped (a band insulator). The alternation of hoppings gives rise to molecular orbitals localized on the nearby sites forming dimers, thereby splitting the QP band into bonding and antibonding subbands. The resulting spectrum has a prominent peak in the occupied part of the spectrum ($\omega < 0$) and a gaplike strong suppression of DOS around the Fermi level [see Figs. 2(b) and 3(c)].

The major observations from the tunneling spectra can thus be consistently understood within this model. In the DW core, two effects dominate: reconstruction of spectra and emergence of the bound state. If the in-gap resonance is disregarded, it can still be observed that the Mott gap is smaller and the DOS distribution is smeared—the behavior reproduced by the intra-DW change of hopping. The in-gap DOS peak at negative bias results from the QP band splitting. The features in the unoccupied part of the spectrum are most likely pushed toward the UHB and are largely submerged into it (see the difference spectra in Fig. 7(b) of Supplemental Material [33]). We also observe a small yet clearly nonzero value of Fermi-level LDOS inside the DW, which results from the subband spectral tails of the split QP band. The spatial distribution of the Fermi-level LDOS and the bound state LDOS are indeed quite similar [see Fig. 2(c)], which confirms their common origin. Finally, the band bending outside the DW is effectively reproduced with the local potential. Its role in metallization is unpronounced inside the DW, even when UHB is brought very close to the Fermi level (see Supplemental Material [33]).

We thus conclude that the structural change in an isolated DW does not yield a good metal in spite of the Mottness collapse. The same result can be extrapolated to the DWs in the hidden state, which have an even larger structural distortion [17,20]. Optical or electrical pulses can, however, affect the orbital structure [65] or cause redistribution of electrons in the Brillouin zone and lead to metallization independent of the density and the type of DWs. Finally, we mention the possibility that the superconductivity in this compound is unrelated to the DWs, and that upon doping, the SC state emerges directly from the quantum spin liquid state; thus $1T - TaS_2$ might be an unconventional resonating-valence-bound superconductor.

We acknowledge the support of the Slovenian Research Agency (ARRS) under P1-0044, J1-7259, and P1-0040, ERC AdG GA 320602 Trajectory, and discussions with Peter Prelovšek, Jernej Mravlje, and Dragan Mihailovic.

[1] E. Tosatti and P. Fazekas, On the nature of the low-temperature phase of $1T - TaS_2$, J. Phys. (Paris), Colloq. **37**, C4-165 (1976).

[2] P. Fazekas and E. Tosatti, Electrical, structural and magnetic properties of pure and doped $1T - TaS_2$, Philos. Mag. B **39**, 229 (1979).

[3] P. Fazekas and E. Tosatti, Charge carrier localization in pure and doped $1T - TaS_2$, Physica (Amsterdam) **99B**, 183 (1980).

[4] R. E. Thomson, U. Walter, E. Ganz, J. Clarke, A. Zettl, P. Rauch, and F. J. DiSalvo, Local charge-density-wave structure in $1T - TaS_2$ determined by scanning tunneling microscopy, Phys. Rev. B **38**, 10734 (1988).

[5] P. W. Anderson, Resonating valence bonds: A new kind of insulator? Mater. Res. Bull. **8**, 153 (1973).

[6] M. Klanjšek, A. Zorko, R. Žitko, J. Mravlje, Z. Jagličić, P. K. Biswas, P. Prelovšek, D. Mihailovic, and D. Arčon, A new high-temperature quantum spin liquid with polaron spins, Nat. Phys. **13**, 1130 (2017).

[7] K. T. Law and P. A. Lee, $1T - TaS_2$ as a quantum spin liquid, Proc. Natl. Acad. Sci. U.S.A. **114**, 6996 (2017).

[8] M. Kratochvilova, A. D. Hillier, A. R. Wildes, L. Wang, S.-W. Cheong, and J. G. Park, The low-temperature highly correlated quantum phase in the charge-density-wave in $1T - TaS_2$, npj Quantum Mater. **2**, 42 (2017).

[9] A. Ribak, I. Silber, C. Baines, K. Chashka, Z. Salman, Y. Dagan, and A. Kanigel, Gapless excitations in the ground state of $1T - TaS_2$, Phys. Rev. B **96**, 195131 (2017).

[10] Y. J. Yu, Y. Xu, L. P. He, M. Kratochvilova, Y. Y. Huang, J. M. Ni, L. Wang, S.-W. Cheong, J.-G. Park, and S. Y. Li, Heat transport study of the spin liquid candidate $1T - TaS_2$, Phys. Rev. B **96**, 081111(R) (2017).

[11] Y. Liu, R. Ang, W. J. Lu, W. H. Song, L. J. Li, and Y. P. Sun, Superconductivity induced by Se-doping in layered charge-density-wave system $1T - TaS_{2-x}Se_x$, Appl. Phys. Lett. **102**, 192602 (2013).

[12] L. J. Li, W. J. Lu, X. D. Zhu, L. S. Ling, Z. Qu, and Y. P. Sun, Fe-doping–induced superconductivity in the charge-density-wave system $1T-TaS_2$, Eurphys. Lett. **97**, 67005 (2012).

[13] B. Sipos, A. F. Kusmartseva, A. Akrap, H. Berger, L. Forró, and E. Tutis, From Mott state to superconductivity in $1T-TaS_2$, Nat. Mater. **7**, 960 (2008).

[14] L. Stojchevska, I. Vaskivskyi, T. Mertelj, P. Kušar, D. Svetin, S. Brazovskii, and D. Mihailović, Ultrafast switching to a stable hidden topologically protected quantum state in an electronic crystal, Science **344**, 177 (2014).

[15] M. Yoshida, R. Suzuki, Y. Zhang, M. Nakano, and Y. Iwasa, Memristive phase switching in two-dimensional $1T-TaS_2$ crystals, Sci. Adv. **1**, e1500606 (2015).

[16] I. Vaskivskyi, I. A. Mihailović, S. Brazovskii, J. Gospodarič, T. Mertelj, D. Svetin, P. Sutar, and D. Mihailovic, Fast electronic resistance switching involving hidden charge density wave states, Nat. Commun. **7**, 11442 (2016).

[17] L. Ma, C. Ye, Y. Yu, X. F. Lu, X. Niu, S. Kim, D. Feng, D. Tománek, Y.-W. Son, X. H. Chen, and Y. Zhang, A metallic mosaic phase and the origin of Mott-insulating state in $1T-TaS_2$, Nat. Commun. **7**, 10956 (2016).

[18] D. Cho, S. Cheon, K.-S. Kim, S.-H. Lee, Y.-H. Cho, S.-W. Cheong, and H. W. Yeom, Nanoscale manipulation of the Mott insulating state coupled to charge order in $1T-TaS_2$, Nat. Commun. **7**, 10453 (2016).

[19] D. Svetin, I. Vaskivskyi, S. Brazovskii, and D. Mihailovic, Three-dimensional resistivity and switching between correlated electronic states in $1T-TaS_2$, Sci. Rep. **7**, 46048 (2017).

[20] Y. A. Gerasimenko, I. Vaskivskyi, and D. Mihailovic, Dual vortex charge order in a metastable state created by an ultrafast topological transition in $1T-TaS_2$, arXiv:1704.08149.

[21] Y. Gerasimenko, I. Vaskivskyi, J. Ravnik, J. Vodeb, V. V. Kabanov, and D. Mihailovic, Ultrafast jamming of electrons into an amorphous entangled state, arXiv:1803.00255.

[22] Y. I. Joe, X. M. Chen, P. Ghaemi, K. D. Finkelstein, G. A. de La Peña, Y. Gan, J. C. T. Lee, S. Yuan, J. Geck, G. J. MacDougall, T. C. Chiang, S. L. Cooper, E. Fradkin, and P. Abbamonte, Emergence of charge density wave domain walls above the superconducting dome in $1T-TiSe_2$, Nat. Phys. **10**, 421 (2014).

[23] S. Yan, D. Iaia, E. Morosan, E. Fradkin, P. Abbamonte, and V. Madhavan, Influence of Domain Walls in the Incommensurate Charge Density Wave State of Cu Intercalated $1T-TiSe_2$, Phys. Rev. Lett. **118**, 106405 (2017).

[24] S. Qiao, X. Li, N. Wang, W. Ruan, C. Ye, P. Cai, Z. Hao, H. Yao, X. Chen, J. Wu, Y. Wang, and Z. Liu, Orbital-Driven Mottness Collapse in $1T-TaS_{2-x}Se_x$ Transition Metal Dichalcogenide, Phys. Rev. X **7**, 041054 (2017).

[25] D. Cho, G. Gye, J. Lee, S.-H. Lee, L. Wang, S.-W. Cheong, and H. W. Yeom, Correlated electronic states at domain walls of a Mott-charge-density-wave insulator $1T-TaS_2$, Nat. Commun. **8**, 392 (2017).

[26] K. Rossnagel, On the origin of charge-density waves in select layered transition-metal dichalcogenides, J. Phys. Condens. Matter **23**, 213001 (2011).

[27] P. Darancet, A. J. Millis, and C. A. Marianetti, Three-dimensional metallic and two-dimensional insulating behavior in octahedral tantalum dichalcogenides, Phys. Rev. B **90**, 045134 (2014).

[28] J.-J. Kim, W. Yamaguchi, T. Hasegawa, and K. Kitazawa, Observation of Mott Localization Gap Using Low Temperature Scanning Tunneling Spectroscopy in Commensuare $1T-TaS_2$, Phys. Rev. Lett. **73**, 2103 (1994).

[29] L. Perfetti, P. A. Loukakos, M. Lisowski, U. Bovensiepen, H. Berger, S. Biermann, P. S. Cornaglia, A. Georges, and M. Wolf, Time Evolution of the Electronic Structure of $1T-TaS_2$ Through the Insulator-Metal Transition, Phys. Rev. Lett. **97**, 067402 (2006).

[30] L. Perfetti, P. A. Loukakos, M. Lisowski, U. Bovensiepen, M. Wolf, H. Berger, S. Biermann, and A. Georges, Femtosecond dynamics of electronic states in the Mott insulator $1T-TaS_2$ by time resolved photoelectron spectroscopy, New J. Phys. **10**, 053019 (2008).

[31] M. Ligges, I. Avigo, D. Golež, H. U. R. Strand, L. Stojchevska, M. Malläne, K. Rossnagel, M. Eckstein, P. Werner, and U. Bovensiepen, Ultrafast Doublon Dynamics in Photo-Excited $1T-TaS_2$, Phys. Rev. Lett. **120**, 166401 (2018).

[32] P. Karpov and S. Brazovskii, Modeling of networks and globules of charged domain walls observed in pump and pulse induced states, Sci. Rep. **8**, 4043 (2018).

[33] See Supplemental Material at http://link.aps.org/supplemental/10.1103/PhysRevLett.122.036802 for discussion of domain-wall types, additional experimental results, description of numerical methods, and additional theory results, which includes Refs. [34–41].

[34] V. Heine, $s-d$ interaction in transition metals, Phys. Rev. **153**, 673 (1967).

[35] K. Rossnagel and N. V. Smith, Spin-orbit coupling in the band structure of reconstructed $1T-TaS_2$, Phys. Rev. B **73**, 073106 (2006).

[36] H. Ishida and A. Liebsch, Embedding approach for dynamical mean-field theory of strongly correlated heterostructures, Phys. Rev. B **79**, 045130 (2009).

[37] H. Ishida and A. Liebsch, Cluster dynamical mean-field study of strongly correlated heterostructures: Correlation-induced reduction of proximity effect, Phys. Rev. B **82**, 045107 (2010).

[38] M. Settnes, S. R. Power, J. Lin, D. H. Petersen, and A.-P. Jauho, Patched Green's function techniques for two-dimensional systems: Electronic behavior of bubbles and perforations in graphene, Phys. Rev. B **91**, 125408 (2015).

[39] M. M. Odashima, B. G. Prado, and E. Vernek, Pedagogical introduction to equilibrium Green's functions: Condensed-matter examples with numerical implementations, Rev. Bras. Ensino Fis. **39**, 1303 (2017).

[40] K. G. Wilson, The renormalization group: Critical phenomena and the Kondo problem, Rev. Mod. Phys. **47**, 773 (1975).

[41] R. Bulla, T. Costi, and T. Pruschke, The numerical renormalization group method for quantum impurity systems, Rev. Mod. Phys. **80**, 395 (2008).

[42] M. Imada, A. Fujimori, and Y. Tokura, Metal-insulator transitions, Rev. Mod. Phys. **70**, 1039 (1998).

[43] F. Gebhardt, *The Mott Metal-Insulator Transition* (Springer, Berlin, 1997).

[44] K. Aryanpour, W. E. Pickett, and R. T. Scalettar, Dynamical mean-field study of the Mott transition in the half-filled

Hubbard model on a triangular lattice, Phys. Rev. B **74**, 085117 (2006).

[45] L. Perfetti, T. A. Gloor, F. Mila, H. Berger, and M. Grioni, Unexpected periodicity in the quasi-two-dimensional Mott insulator $1T-TaS_2$ revealed by angle-resolved photoemission, Phys. Rev. B **71**, 153101 (2005).

[46] J. K. Freericks, H. R. Krishnamurthy, Y. Ge, A. Y. Liu, and Th. Pruschke, Theoretical description of time-resolved pump/probe photoemission in TaS_2: A single-band DFT +DMFT(NRG) study within the quasiequilibrium approximation, Phys. Status Solidi B **246**, 948 (2009).

[47] T. Yoshioka, A. Koga, and N. Kawakami, Quantum Phase Transitions in the Hubbard Model on a Triangular Lattice, Phys. Rev. Lett. **103**, 036401 (2009).

[48] T. Shirakawa, T. Tohyama, J. Kokalj, S. Sota, and S. Yunoki, Ground-state phase diagram of the triangular lattice Hubbard model by the density-matrix renormalization group method, Phys. Rev. B **96**, 205130 (2017).

[49] A. Georges, G. Kotliar, W. Krauth, and M. J. Rozenberg, Dynamical mean-field theory of strongly correlated fermion systems and the limit of infinite dimensions, Rev. Mod. Phys. **68**, 13 (1996).

[50] M. Potthoff and W. Nolting, Surface metal-insulator transition in the Hubbard model, Phys. Rev. B **59**, 2549 (1999).

[51] M. Potthoff and W. Nolting, Metallic surface of a Mott insulator–Mott insulating surface of a metal, Phys. Rev. B **60**, 7834 (1999).

[52] M. Potthoff and W. Nolting, Dynamical mean-field study of the Mott transition in thin films, Eur. Phys. J. B **8**, 555 (1999).

[53] J. K. Freericks, Dynamical mean-field theory for strongly correlated inhomogeneous multilayered nanostructures, Phys. Rev. B **70**, 195342 (2004).

[54] J. Freericks, *Transport in Multilayered Nanostructures: The Dynamical Mean-field Theory Approach* (Imperial College Press, London, 2006).

[55] S. Okamoto and A. J. Millis, Spatial inhomogeneity and strong correlation physics: A dynamical mean-field study of a model Mott-insulator–band-insulator heterostructure, Phys. Rev. B **70**, 241104(R) (2004).

[56] R. W. Helmes, T. A. Costi, and A. Rosch, Kondo Proximity Effect: How Does a Metal Penetrate into a Mott Insulator?, Phys. Rev. Lett. **101**, 066802 (2008).

[57] M. Jiang, G. G. Batrouni, and R. T. Scalettar, Density of states and magnetic correlations at a metal-Mott insulator interface, Phys. Rev. B **86**, 195117 (2012).

[58] J. Lee and C.-H. Yee, Interfaces in coexisting metals and Mott insulators, Phys. Rev. B **95**, 205126 (2017).

[59] P. Bakalov, D. N. Esfahani, L. Covaci, F. M. Peeters, J. Tempere, and J.-P. Locquet, Electric-field-driven Mott metal-insulator transition in correlated thin films: An inhomogeneous dynamical mean-field theory approach, Phys. Rev. B **93**, 165112 (2016).

[60] A. Georges and W. Krauth, Numerical Solution of the $d=\infty$ Hubbard Model: Evidence for a Mott Transition, Phys. Rev. Lett. **69**, 1240 (1992).

[61] X. Y. Zhang, M. J. Rozenberg, and G. Kotliar, Mott Transition in the $d=\infty$ Hubbard Model at Zero Temperature, Phys. Rev. Lett. **70**, 1666 (1993).

[62] P. Werner and A. J. Millis, Doping-driven Mott transition in the one-band Hubbard model, Phys. Rev. B **75**, 085108 (2007).

[63] R. Žitko, D. Hansen, E. Perepelitsky, J. Mravlje, A. Georges, and B. S. Shastry, Extremely correlated Fermi liquid theory meets dynamical mean-field theory: Analytical insights into the doping-driven Mott transition, Phys. Rev. B **88**, 235132 (2013).

[64] D. E. Logan and M. R. Galpin, Mott insulators and the doping-induced Mott transition within DMFT: Exact results for the one-band Hubbard model, J. Phys. Condens. Matter **28**, 025601 (2016).

[65] T. Ritschel, J. Trinckauf, K. Koepernik, B. Buchner, M. von Zimmermann, H. Berger, Y. I. Joe, P. Abbamonte, and J. Geck, Orbital textures and charge density waves in transition metal dichalcogenides, Nat. Phys. **11**, 328 (2015).